Double-layer buffer template to grow commensurate epitaxial $BaBiO_3$ thin films

Han Gyeol Lee, Yoonkoo Kim, Sangwoon Hwang, Gideok Kim, Tae Dong Kang, Minu Kim, Miyoung Kim, and Tae Won Noh

Citation: APL Mater. **4**, 126106 (2016); doi: 10.1063/1.4972133
View online: http://dx.doi.org/10.1063/1.4972133
View Table of Contents: http://aip.scitation.org/toc/apm/4/12
Published by the American Institute of Physics

Double-layer buffer template to grow commensurate epitaxial $BaBiO_3$ thin films

Han Gyeol Lee,[1,2] Yoonkoo Kim,[3] Sangwoon Hwang,[3] Gideok Kim,[1,2] Tae Dong Kang,[1,2] Minu Kim,[1,2,a] Miyoung Kim,[3] and Tae Won Noh[1,2,a]
[1]*Center for Correlated Electron Systems, Institute for Basic Science (IBS), Seoul 08826, South Korea*
[2]*Department of Physics and Astronomy, Seoul National University (SNU), Seoul 08826, South Korea*
[3]*Department of Materials Science and Engineering, Seoul National University (SNU), Seoul 08826, South Korea*

(Received 1 September 2016; accepted 29 November 2016; published online 19 December 2016)

We propose a $BaCeO_3/BaZrO_3$ double-layer buffer template, grown on a $SrTiO_3$ substrate, for epitaxial growth of a target oxide film with large lattice constants of over 4.1 Å. Lattice mismatch from the substrate was mostly accommodated for by a $BaZrO_3$ arbitrating layer. Having an ideal in-plane lattice structure, $BaCeO_3$ served as the main-buffer to grow the target material. We demonstrated commensurate epitaxy of $BaBiO_3$ (BBO, a = 4.371 Å) utilizing the new buffer template. Our results can be applied to heteroepitaxy and strain engineering of novel oxide materials of sizable lattice constants. [http://dx.doi.org/10.1063/1.4972133]

There has been extensive research in strain engineering directed towards tuning the material properties of oxide thin films by applying biaxial strain. Most bulk oxides are fairly brittle, and will develop cracks under temperate strain (~0.1%).[1] However, it is possible to impose commensurate elastic strain on oxide thin films up to a few percent through the use of epitaxy and misfit strain imposed by the substrate. These strain engineering approaches have been particularly useful for films with perovskite oxides of the form ABO_3 (A is a rare earth or alkali metal, B is a transition metal or post-transition metal, and O is oxygen). The simple crystal structures of these perovskite oxides allow for easy growth of high-quality commensurate films using heteroepitaxy. Thus, strain engineering of perovskite oxide films has been widely used to alter band structures[2] and significantly enhance superconducting,[3] ferromagnetic,[4] and ferroelectric properties.[5]

Recently, several perovskite oxides of large lattice constants (i.e., a > 4.1 Å) have received much attention. For example, the field-induced ferro-antiferroelectric transition in $PbZrO_3$ (a = 4.152 Å)[6] and the transparent high-mobility semiconductor $BaSnO_3$ (a = 4.116 Å)[7] have been investigated as new platforms for studying versatile physical properties and functionalities. Additionally, the colossal ionic conductivity in both Y-doped $BaZrO_3$ (a > 4.1 Å)[8] and in $BaCeO_3$ (a > 4.15 Å),[9] at relatively low temperatures, is a fast-growing subject in solid oxide fuel cell research. Another notable example is $BaBiO_3$ (BBO, $a_{\text{pseudo-cubic}}$ = 4.371 Å),[10] which is well-known for being the mother compound of the high-T_c superconductors, $Ba_{1-x}K_xBiO_3$ (T_c = 34 K)[11] and $BaPb_xBi_{1-x}O_3$ (T_c = 13 K).[12] In addition, it has recently been predicted that electron-doped BBO is an oxide topological insulator, resulting from strong spin-orbit coupling of Bi.[13,14] Thus, strain engineering is an important tool for observing novel physical properties of materials with large lattice constants.

However, it has been difficult to identify suitable substrates for growing these perovskite oxides in commensurate epitaxial films. Most commercially available perovskite oxide substrates have lattice constants between 3.7 and 4.0 Å.[15] We note that rare earth scandates[16] ($a_{\text{pseudo-cubic}}$ ~ 4.0 Å) and

[a]Authors to whom correspondence should be addressed. Electronic mail: minukim@fkf.mpg.de and twnoh@snu.ac.kr

luthethates[17] ($a_{\text{pseudo-cubic}} \sim 4.2$ Å) have been developed successfully, providing substrates of higher lattice constants. However, these substrates still suffer from lattice twinning problems due to their orthorhombic structures, which is a significant obstacle for commensurate growth. Furthermore, these substrates are generally in short supply due to the limited growth of single crystals. On the other hand, $SrTiO_3$ (STO, $a = 3.905$ Å) is commercially available and has a simple cubic structure. Therefore, we found it beneficial to develop a suitable template for growing large oxides by utilizing commercial STO substrates.

In this paper, we adopt a strategy that uses buffer layers to obtain commensurate epitaxial BBO films on STO substrates, whose lattice mismatch is about 11.9%. This buffer layer technique has been used previously to alleviate large lattice mismatch.[18–20] For example, growth of high-quality GaN[18] and ZnO[19] on Al_2O_3 substrates was realized by overcoming a mismatch problem through the use of buffer layers. Here, we utilize a template composed of two buffer layers:[20] an arbitrating layer and a main-buffer layer. The main-buffer layer is used to provide a desired commensurable lattice for the target material (BBO), with a lattice mismatch of less than a few percent. For this purpose, we use $BaCeO_3$ (BCO, $a = 8.777$ Å, $b = 6.236$ Å, and $c = 6.216$ Å; orthorhombic in bulk)[21] because of the small lattice mismatch between BBO and BCO (0.43%), in the pseudo-cubic notation. However, there remains a lattice mismatch between BCO and STO, of 12.4%. To obtain a high-quality BCO layer, it is necessary to insert an arbitrating layer between the BCO main-buffer layer and the STO substrate. We use $BaZrO_3$ (BZO, $a = 4.192$ Å; cubic in bulk) as the arbitrating material.[22] With the intermediate lattice constant of the arbitrating material, lying between those of BCO and STO, we are able to circumvent obstacles due to the very large lattice mismatch.

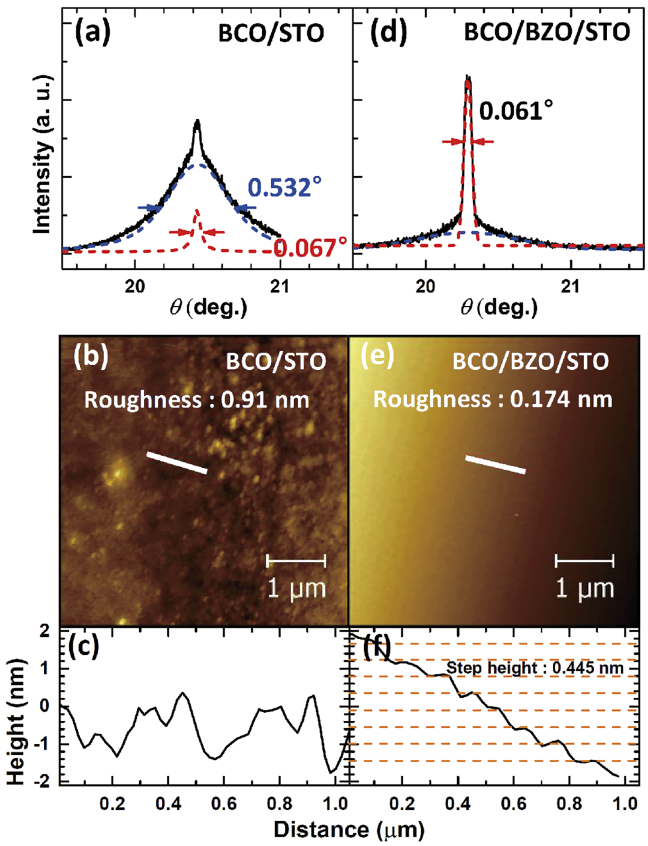

FIG. 1. X-ray diffraction (XRD) rocking curve for (002) diffraction of $BaCeO_3$ (BCO) layers on (a) the $SrTiO_3$ (STO) substrate and (d) the $BaZrO_3$ (BZO) arbitrating layer. Red and blue dashed lines are a Gaussian component and background component of raw data. Arrows indicate full-width at half maximum values of fitting curves. The pseudo-cubic notation was used for indexing all reflections. Atomic force microscopy (AFM) topographic images of the BCO layers on (b) the STO substrate and (e) the BZO arbitrating layer. A line profile along the white line in (b) was plotted in (c), and a profile along the line in (e) was plotted in (f).

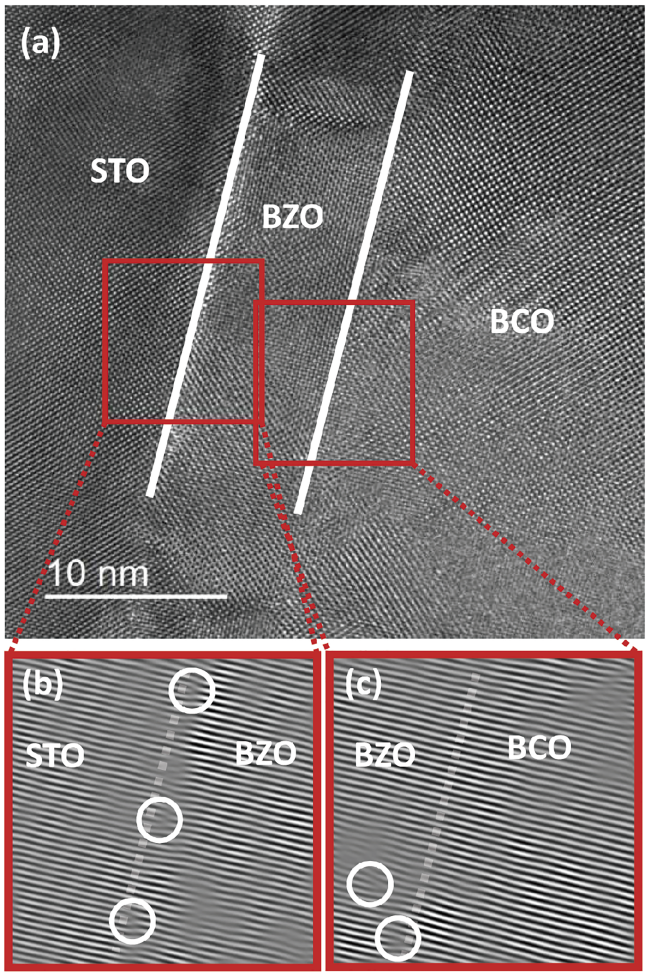

FIG. 2. (a) High-resolution transmission electron microscopy (HRTEM) image of the double-layer buffer structure on the STO substrate. (b) and (c) Fourier-filtered images of the red squares in (a), using the (100) location. The white circles indicate the positions of misfit dislocations, and the white lines indicate the interfaces between layers.

We fabricated BBO films, as well as associated BCO/BZO heterostructures, using pulsed laser deposition. We used commercially available STO (001) substrates (Shinkosha, Kanagawa, Japan) that were chemically and thermally pretreated to obtain atomically flat surfaces. The substrates were put into a vacuum chamber (base pressure $\sim 10^{-9}$ Torr; PASCAL, Osaka, Japan) and pre-annealed at 950 °C for 30 min in a 5×10^{-6} Torr oxygen environment. Atomic force microscopy (AFM; Asylum Research, Santa Clara, CA, USA) independently confirmed that this pre-annealing process made the STO (001) surfaces atomically flat. After pre-annealing, we increased the oxygen gas pressure to 100 mTorr and heated the substrates. Using a KrF excimer laser ($\lambda = 248$ nm; Coherent, Santa Clara, CA, USA), we ablated targets at a laser fluence of 0.6 J/cm^2. The growth temperature was 500 °C for BBO and BZO layers, and 750 °C for the BCO layer. The structures of grown films were examined using high-resolution X-ray diffraction (HR-XRD) ($\lambda = 0.154056$ nm; Bruker, Karlsruhe, Germany), and their surface morphologies were studied using AFM. The microstructure of each layer, as well as dislocations near the interfaces, was examined by a high-resolution transmission electron microscope (TEM; JEOL, Peabody, MA, USA).

When we attempted to grow a single BCO layer on the STO, the large lattice mismatch of 12.4% made it difficult to obtain a high-quality crystalline structure. As shown in Fig. 1(a), the XRD rocking curve of a 12 nm-thick BCO layer shows a very broad feature, indicative of the mosaicity spread in crystal structure.[23] The large full width at half-maximum (FWHM) value of the broad feature indicates a huge lattice plane inclination.[24] The rocking curve exhibits a small Gaussian component

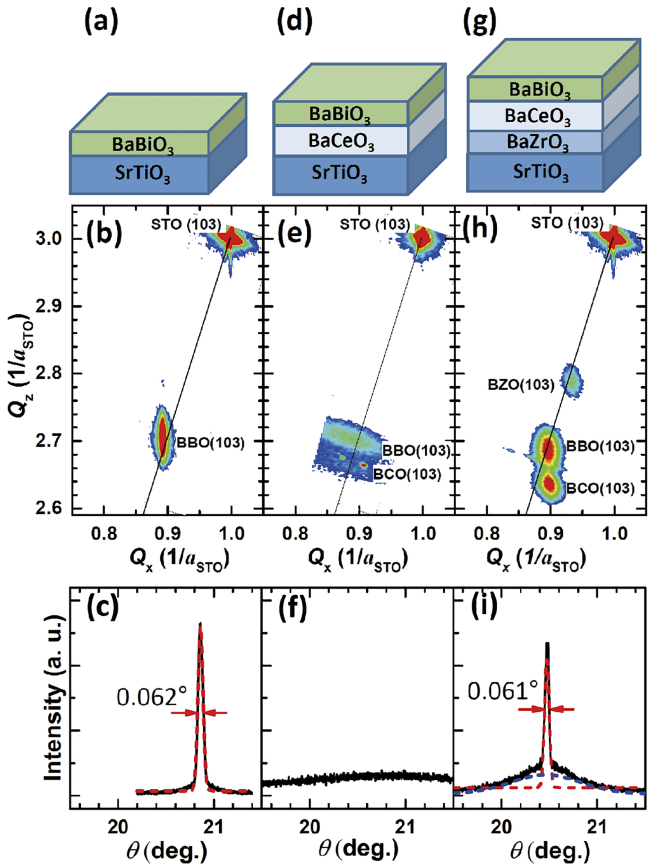

FIG. 3. Schematic sample structures of (a) BBO/STO, (d) BBO/BCO/STO, and (g) BBO/BCO/BZO/STO. (b), (e), and (h) Reciprocal space maps (RSMs) around STO (103) diffraction measured from (a), (d), and (g), respectively. The black lines are cubic relaxation lines from STO (103). (c), (f), and (i) XRD rocking curves at BBO (002) diffraction from (a), (d), and (g), respectively. Red and blue dashed lines are a Gaussian component and background component of raw data. Arrows indicate full-width at half maximum values of rocking curves. The pseudo-cubic notation was used for indexing all reflections.

which indicates the existence of a crystallized region with a small volume, but large mosaicity spread made it unsuitable for use as a buffer template. This degradation of crystallinity was also observed as polycrystalline domains in a TEM image (not shown). The AFM image in Fig. 1(b) shows a surface with a high roughness value of 0.91 nm. The line profile along the white line in Fig. 1(c) shows large fluctuations in height.

On the other hand, we were able to grow a high-quality BCO layer (thickness of 12 nm) on STO using a 10 nm-thick BZO arbitrating layer. This double-layer structure has a sharp rocking curve for the BCO layer, with a small FWHM value of 0.061° [Fig. 1(d)]. This suggests that the mosaicity problem could be overcome by using a BZO arbitrating layer. Furthermore, the surface roughness is significantly less, at about 0.174 nm [Fig. 1(e)]. The line profile along the BCO surface shows a step-and-terrace pattern [Fig. 1(f)]. The height of each step is ~0.44 nm, within the experimental resolution of AFM. This height value is consistent with the known out-of-plane lattice constant of the BCO film, and is confirmed by XRD measurements.

The growth of a high-quality BCO layer in the BCO/BZO/STO heterostructure is made possible due to the high density of accommodated misfit dislocations in the BZO layer. Fig. 2(a) shows a HRTEM image of the BCO/BZO/STO heterostructure. This image reveals well-defined sharp interfaces and epitaxial growth of thin films. Fourier-filtered images of the two red square areas [Figs. 2(b) and 2(c)] reveal several edge dislocations near the interfaces; the white circles in Fig. 2(b) indicate edge dislocations near the interface between STO and BZO layers, and Fig. 2(c) shows two dislocations appearing at the BZO/BCO interface and in the BZO layer. This indicates that strain relaxation occurred throughout the high density of misfit dislocations inside the intermediate BZO

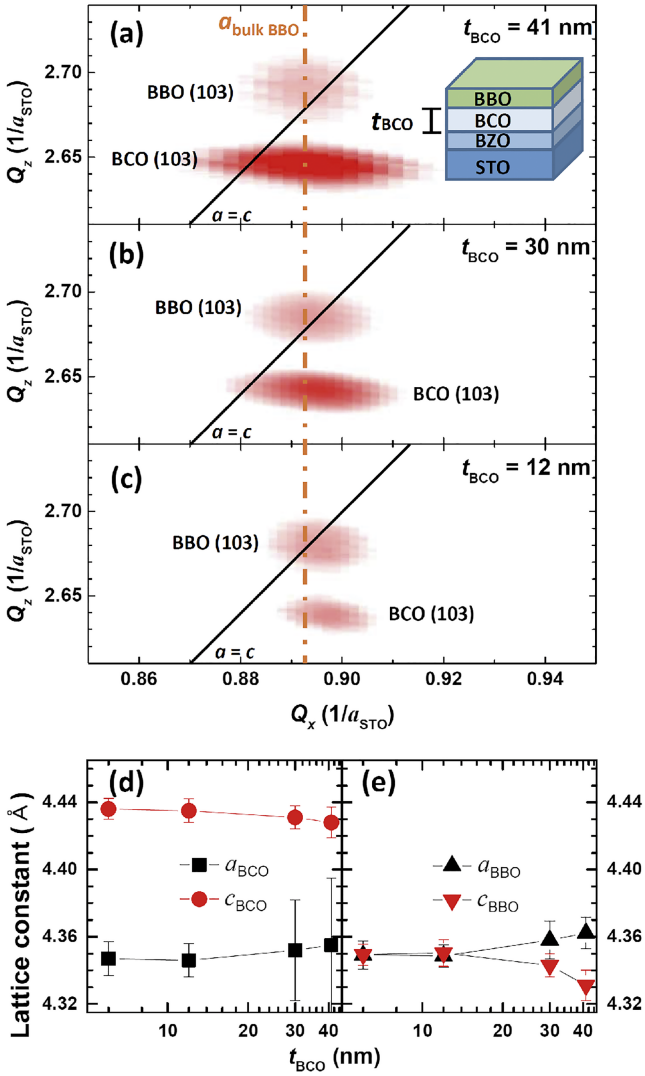

FIG. 4. (a)–(c) RSMs around STO (103) diffraction measured from BBO/BCO/BZO/STO structures of differing BCO thicknesses (t_{BCO}). The orange dashed line is the reciprocal position of the in-plane lattice constant of a fully relaxed BBO thin film (tetragonal). The solid black lines are cubic relaxation lines of the STO (103). (d) and (e) Lattice constants (a and c) of the BCO and BBO layers, for differing t_{BCO}. The pseudo-cubic notation was used for indexing all reflections.

layer. It is important to note that there was little dislocation within the BCO layer, thus providing us with an ideal platform for growing target materials as commensurate epitaxial films.

The BCO/BZO double-layer buffer structure enables the growth of high-quality commensurate epitaxial BBO films. Fig. 3 shows sample geometry and XRD results of three different BBO structures: BBO/STO, BBO/BCO/STO, and BBO/BCO/BZO/STO. As previously reported,[25] BBO thin films can be grown directly on STO substrates, but only in a fully relaxed state [Figs. 3(a)–3(c)]. When only a single BCO buffer layer was used, the quality of both the BCO buffer and the BBO thin film was seriously degraded [Figs. 3(d)–3(f)]. This was due to the large mosaicity and associated defects in the BCO layer. On the other hand, the BBO layer on the double-layer buffer structure received epitaxial strain from the BCO layer. As shown in the reciprocal space map (RSM) of Fig. 3(h), the in-plane peak position of the BBO is aligned with that of the BCO, suggesting that the BBO layer was commensurately grown and fully strained (0.48%) against the BCO layer. The XRD rocking curve in Fig. 3(i) shows small mosaicity spread (blue line), but a large volume of the well-crystallized region (red line) compared with the single buffered sample.

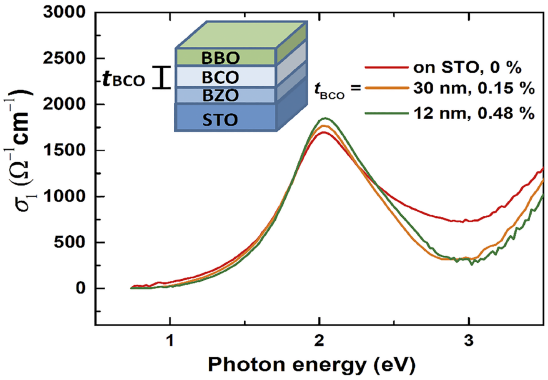

FIG. 5. Optical conductivity spectra of BBO films: in the commensurate states on BCO/BZO/STO (the orange and the green lines), and in the fully relaxed state on STO (the red line). Biaxial compressive strains (%) for each structure are given.

In addition, we confirmed the commensurate epitaxial growth of the BBO thin film by varying the thickness of the BCO layer (t_{BCO}). Figs. 4(a)–4(c) show the RSM of BBO (103) and BCO (103) peaks for three different BBO films. In our buffer structure, partial compressive strain was imposed on the BCO sublayer by the BZO sublayer. The partial strain relaxation was dependent on t_{BCO}. By decreasing t_{BCO}, the BCO (103) peak moved to the right, indicating that a larger compressive strain was imposed. The in-plane peak broadening of the BCO layer was evidence of partial strain relaxation due to the change in thickness. The experimental values of in-plane (a) and out-of-plane (c) lattice constants are shown in Figs. 4(d) and 4(e), for BCO and BBO layers, respectively. As t_{BCO} was decreased, a_{BCO} and a_{BBO} decreased, while c_{BCO} and c_{BBO} increased. Moreover, the change in a_{BBO} was the same as that of a_{BCO}, indicating that the BBO thin film was epitaxially grown on the BCO sublayer.

We measured the optical conductivity spectra $\sigma_1(\omega)$ of BBO films grown on BCO/BZO/STO, as well as ones grown directly on STO substrates, using spectroscopic ellipsometry. As shown in Fig. 5, all of the BBO films exhibit a 2.0 eV peak in $\sigma_1(\omega)$. This peak has been attributed to charge density wave (CDW) instability, which is coupled to breathing mode distortions of the BiO_6 octahedra.[26–28] Note that BBO films grown on the BCO/BZO/STO buffer structure all have very similar $\sigma_1(\omega)$, independent of sublayer thickness and applied strain. Thus, our buffer structure is a reliable template since the buffered films did not lose their original property.[29,30]

In summary, we used a double-layer buffer structure to obtain epitaxial growth of BBO thin films on STO substrates, with a large lattice mismatch of about 11.9%. The BZO arbitrating layer accommodated for the large lattice mismatch from the STO, by generating high-density misfit dislocations. Additionally, the BCO main-buffer layer could be used to impart commensurate strain on the target perovskite film. As a result, we successfully achieved commensurate epitaxial growth of BBO films using the double-layer buffer. These results indicate that the BCO/BZO double-layer buffer structure may be useful for the growth of various other oxide materials of large lattice constant (>4.1 Å) (see the supplementary material). By replacing the main-buffer layer with one made of a different material [i.e., $BaPbO_3$ (a = 4.265 Å) or $BaTbO_3$ (a = 4.285 Å)] this double-layer buffer template can be applied in the strain engineering of various perovskite oxides.

See supplementary material for the atomic-resolved TEM image of the BZO arbitrating layer, the AFM image of the BBO surface, and another application of the double-layer buffer template.

This work was supported by IBS-R009-D1. We would like to thank Seung Chul Chae and Hodong Lee for their help with the experiments and helpful discussions.

[1] D. G. Schlom, L.-Q. Chen, C. J. Fennie, V. Gopalan, D. A. Muller, X. Pan, R. Ramesh, and R. Uecker, MRS Bull. **39**, 118 (2014).
[2] S. J. May, J.-W. Kim, J. M. Rondinelli, E. Karapetrova, N. A. Spaldin, A. Bhattacharya, and P. J. Ryan, Phys. Rev. B **82**, 014110 (2010).
[3] H. Sato and M. Naito, Physica C **274**, 221 (1997).
[4] W. Lu, W. Song, P. Yang, J. Ding, G. M. Chow, and J. Chen, Sci. Rep. **5**, 10245 (2015).

[5] K. J. Choi, M. Biegalski, Y. L. Li, A. Sharan, J. Schubert, R. Uecker, P. Reiche, Y. B. Chen, X. Pan, V. Gopalan, L.-Q. Chen, D. G. Schlom, and C. B. Eom, Science **306**, 1005 (2004).
[6] T. Tani, J. F. Li, D. Viehland, and D. A. Payne, J. Appl. Phys. **75**, 3017 (1994).
[7] H. J. Kim, U. Kim, H. M. Kim, T. H. Kim, H. S. Mun, B. G. Jeon, K. T. Hong, W. J. Lee, C. Ju, K. H. Kim, and K. Char, Appl. Phys. Express **5**, 061102 (2012).
[8] L. Bi, S. P. Shafi, and E. Traversa, J. Mater. Chem. **3**, 5815 (2015).
[9] K. Takeuchi, C.-K. Loong, J. W. Richardson, Jr., J. Guan, S. E. Dorris, and U. Balachandran, Solid State Ionics **138**, 63 (2000).
[10] A. W. Sleight, Physica C **514**, 152 (2015).
[11] A. W. Sleight, J. L. Gillson, and P. E. Bierstedt, Solid State Commun. **17**, 27 (1975).
[12] R. J. Cava, B. Batlogg, J. J. Krajewski, R. Farrow, L. W. Rupp, Jr., A. E. White, K. Short, W. F. Peck, and T. Kometani, Nature **332**, 814 (1988).
[13] D. Xiao, W. Zhu, Y. Ran, N. Nagaosa, and S. Okamoto, Nat. Commun. **2**, 596 (2011).
[14] B. Yan, M. Jansen, and C. Felser, Nat. Phys. **9**, 709 (2013).
[15] D. G. Schlom, L.-Q. Chen, X. Pan, A. Schmehl, and M. A. Zurbuchen, J. Am. Ceram. Soc. **91**, 2429 (2008).
[16] R. Uecker, B. Velickov, D. Klimm, R. Bertram, M. Bernhagen, M. Rabe, M. Albrecht, R. Fornari, and D. G. Schlom, J. Cryst. Growth **310**, 2649 (2008).
[17] K. L. Ovanesyan, A. G. Petrosyan, G. O. Shirinyan, C. Pedrini, and L. Zhang, J. Cryst. Growth **198**, 497 (1999).
[18] H. Amano, N. Sawaki, I. Akasaki, and Y. Toyoda, Appl. Phys. Lett. **48**, 353 (1986).
[19] Y. Chen, S. K. Hong, H. J. Ko, V. Kirshner, H. Wenisch, T. Yao, K. Inaba, and Y. Segawa, Appl. Phys. Lett. **78**, 3352 (2001).
[20] K. Terai, M. Lippmaa, P. Ahmet, T. Chikyow, T. Fujii, H. Koinuma, and M. Kawasaki, Appl. Phys. Lett. **80**, 4437 (2002).
[21] K. S. Knight, Solid State Ionics **74**, 109 (1994).
[22] A. R. Akbarzadeh, I. Kornev, C. Malibert, L. Bellaiche, and J. M. Kiat, Phys. Rev. B **72**, 205104 (2005).
[23] R. Chierchia, T. Böttcher, H. Heinke, S. Einfeldt, S. Figge, and D. Hommel, J. Appl. Phys. **93**, 8918 (2003).
[24] P. E. Janolin, A. S. Anokhin, Z. Gui, V. M. Mukhortov, Y. I. Golovko, N. Guiblin, S. Ravy, M. E. Marssi, Y. I. Yuzyuk, L. Bellaiche, and B. Dkhil, J. Phys.: Condens. Matter **26**, 292201 (2014).
[25] G. Kim, M. Neumann, M. Kim, M. D. Le, T. D. Kang, and T. W. Noh, Phys. Rev. Lett. **115**, 226402 (2015).
[26] D. E. Cox and A. W. Sleight, Solid State Commun. **19**, 969 (1976).
[27] D. Korotin, D. Novoselov, and V. I. Anisimov, J. Phys.: Condens. Matter **24**, 415603 (2012).
[28] Z. P. Yin, A. Kutepov, and G. Kotliar, Phys. Rev. X **3**, 021011 (2013).
[29] R. P. S. M. Lobo and F. Gervais, Phys. Rev. B **52**, 13294 (1995).
[30] T. Nishio, J. Ahmad, and H. Uwe, Phys. Rev. Lett. **95**, 176403 (2005).